# MACHINE LEARNING IN FUNDAMENTAL PHYSICS

# Filtering of false EAS maxima using neural network methods in the SPHERE-3 experiment

E.L. Entina,<sup>1,\*</sup> D.A. Podgrudkov,<sup>1,2,†</sup> T.A. Kolodkin,<sup>1,2</sup>
E.A. Bonvech,<sup>1</sup> O.V. Cherkesova,<sup>1,3</sup> D.V. Chernov,<sup>1</sup> V.I. Galkin,<sup>1,2</sup>
V.A. Ivanov,<sup>1,2</sup> N.O. Ovcharenko,<sup>1,2</sup> T.M. Roganova,<sup>1</sup> and M.D. Ziva<sup>1,4</sup>

<sup>1</sup>Skobeltsyn Institute of Nuclear Physics Lomonosov Moscow State University

<sup>2</sup>Lomonosov Moscow State University, Faculty of Physics

<sup>3</sup>Lomonosov Moscow State University, Department of Cosmic Research

<sup>4</sup>Lomonosov Moscow State University, Faculty of Computational Mathematics and Cybernetics

(Received xx.xx.2025; Revised xx.xx.2025; Accepted xx.xx.2025)

The 9th International Conference in Deep Learning in Computational Physics

Abstract

The SPHERE-3 telescope, currently under development, is designed to study cosmic rays in the energy

range of 1–1000 PeV. In this work, we propose a method for filtering extensive air shower (EAS) events

whose axes lie outside the telescope's field of view by employing two complementary machine learning

approaches. The first approach uses a convolutional neural network (CNN) to regress the distance

between the telescope axis and the EAS axis. The second relies on an autoencoder with an embedded

spatial transformer network, trained to reconstruct only 'true' EAS images and to discriminate events

based on reconstruction error. We demonstrate that the combined approach achieves high accuracy:

most 'true' events are retained while 'false' ones are effectively suppressed.

Since the method does not depend on the primary particle's energy, mass, or arrival direction, it

provides robust and universal filtering. The method can be integrated into a trigger system or event

selection pipeline for subsequent physical analysis.

PACS numbers: 07.05.Mh, 07.05.Pj, 96.50.S-, 96.50.sd

Keywords: Convolutional neural network, Autoencoders, Cherenkov light, cosmic rays

INTRODUCTION

The SPHERE-3 telescope, currently under design, is intended to study cosmic rays with

energies ranging from 1 to 1000 PeV. The telescope will register Vavilov-Cherenkov radiation

(Cherenkov light, CL) reflected from a snow surface in order to accomplish this goal. One of

the key steps in data processing is the correct identification of events in which the axis of an

extensive air shower (EAS) falls within the telescope's field of view (FOV), or more precisely,

within its fiducial area.

In every experiment, a specific set of conditions must be satisfied for an event to be accepted

for analysis. One of these conditions is the location of the shower axis within a certain area

(spacial or angular). Typically, this region is fully contained within the detector's geometrical

area (or full FOV) and might be smaller. For conventional large-scale EAS detector arrays, it

is typical to step one or two stations from the border of the array [1, 2]. For smaller arrays,

the selection criteria typically requires that the reconstructed EAS axis lies within the detector

\* E-mail: el.entina@physics.msu.ru

† E-mail: d.a.podgrudkov@physics.msu.ru

x-2

perimeter [3].

At large distances between the EAS axis and the center of the FOV, fluctuations can create situations, in which the apparent bright spot does not accurately correspond to the actual position of the EAS axis, especially in case of near-edge axes location. This can lead to systematic errors when reconstructing the properties of the primary particle based on an approximation of the photons lateral distribution function.

To improve the quality of data analysis, filtering of such 'false' events is necessary. Correct identification of images in which the brightness maximum corresponds to the true position of the EAS axis reduces systematic uncertainties and enhances the reliability of subsequent physical analyses. This work proposes a method for filtering such events, based on the use of machine learning algorithms specifically trained on simulated images, achieving high accuracy in distinguishing true and false maxima, independent of the energy, mass, and angle of arrival of the primary particle.

The SPHERE-3 experiment setup is presented in Fig. 1. The telescope with a 20° field of view is mounted on an unmanned aerial platform with flight altitudes ranging from 500 to 1500 meters above the snow covered surface. The telescope's sensitive camera has 379 optical segments, each housing 7 silicone photomultipliers (SiPM) with lens light collectors, 2563 pixels in total. The detector's effective aperture is about 2 m<sup>2</sup> [4]. This configuration allows for detecting of EAS CL reflected from the surface in the energy range of the primary particle from 1 to 1000 PeV. The geometry of the experiment defines a critical zone: as the shower axis moves away from the center of the field of view, the image gradually moves out of the observable region. For each height, there exists a radius beyond which the axis is no longer under direct observation.

#### 2. BACKGROUND AND RELATED WORK

# Methods for reconstructing EAS primary particle parameters

Various techniques have been developed to reconstruct the primary parameters of EAS. Ground-based particle arrays, such as the Pierre Auger Observatory and the Telescope Array, employ networks of scintillation or water-Cherenkov detectors to measure the density of secondary particles at the ground. In contrast, imaging atmospheric Cherenkov telescopes (IACTs) detect the direct Cherenkov light emitted in the atmosphere. Some arrays combine optical and particle measurements to extend the effective area, though they require large infrastructures. The SPHERE concept offers an alternative, enabling such studies with a single, compact instru-

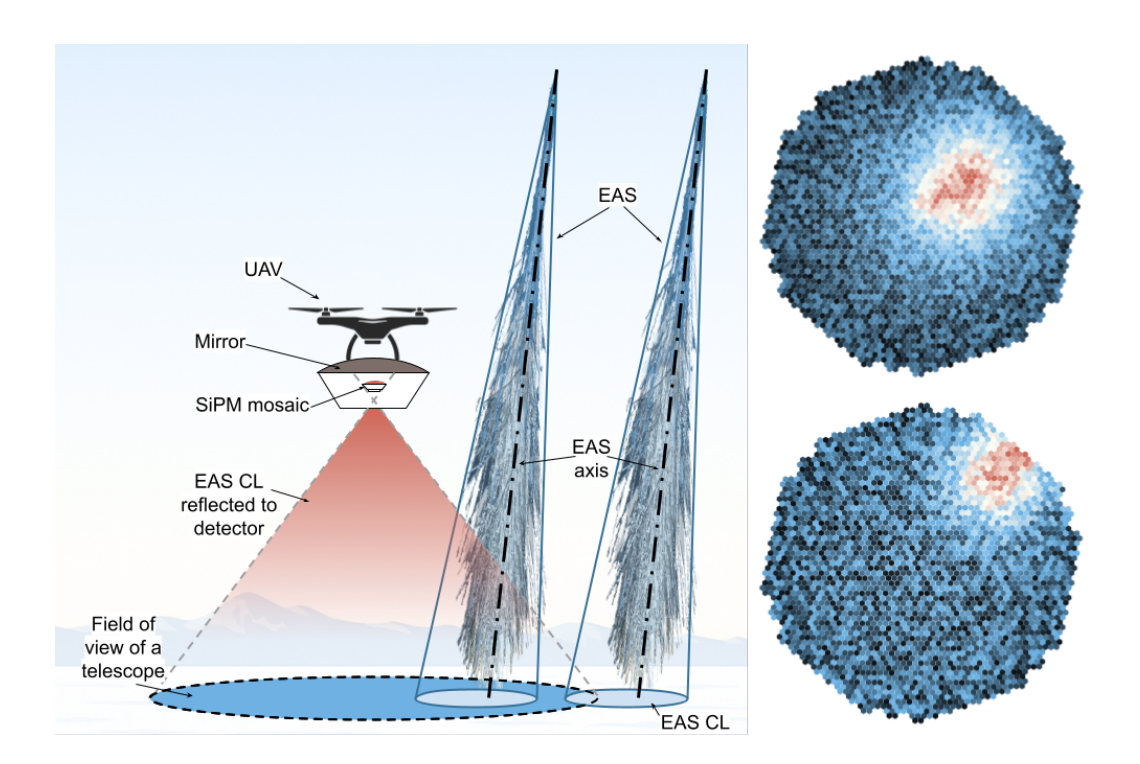


Figure 1. SPHERE-3 Experiment Scheme. On the left is a schematic representation of the experimental setup, on the right is a schematic representation of the EAS events, whose axis fell inside and outside the field of view boundary. The images are conceptual and not based on actual data or simulations.

ment by detecting Cherenkov light reflected from a snow surface using a telescope carried on a balloon or unmanned platform. This method provides information close to the shower core with minimal hardware, though it introduces specific systematic effects.

#### The SPHERE Series

The technique of detecting Cherenkov light from extensive air showers via reflection from a snow surface has been explored in the SPHERE program and related efforts for decades. Balloon-borne SPHERE-2 [5] measurements performed in 2011–2013 demonstrated the feasibility of the approach and provided both simulated and experimental constraints on reconstruction accuracy and systematic effects for reflected Cherenkov observations [6].

Our recent studies were focused on modeling and improving the methodology for reflectedlight telescopes. In particular, modelling efforts developed for SPHERE-3 indicate enhanced angular and photometric sensitivity compared to earlier prototypes.

## Status of SPHERE-3 and origin of the 'false maxima' concern

The SPHERE-3 detector is currently in the design and simulation stage and has not yet acquired real data; therefore, the present paper and related performance estimates are based on detailed simulations.

Simulation studies provide the primary evidence that local fluctuations can produce a brightest pixel (a local maximum) that does not correspond to the true projection of the shower axis. Independent work within the collaboration has explicitly examined the impact of filtering out these 'false maxima' on the reconstructed primary parameters, showing that such filtering can significantly alter the estimated energy and composition distributions in model-based studies. In particular, the [7] presents a method for filtering and quantifies how the results change depending on the accuracy of the filtering process, using simulated events for their analysis. Similar to this study, our research was conducted on simulated events using a software suite [8].

#### 3. THE PROBLEM OF 'FALSE' MAXIMA

Registration of events near or outside the FOV boundary leads to a specific problem. Methods for recovering primary parameters based on approximating the CL photons distribution assume that the brightness maximum of the image corresponds to the projection of the shower axis. However, in the case of partial observation of the EAS, the brightness maximum may be caused by local fluctuations of the cascade and be shifted towards the edge of the image, not coinciding with the true axis. Using such 'false' maxima in the reconstruction of primary particle parameters leads to systematic errors, particularly when estimating the energy distribution.

The traditional method, also described in [7], is based on constructing some feature extraction function (a function that yields a value using all pixels' data), the distribution of which should differ for true and false events (i.e. the  $\chi^2$  of the best-fit axial-symmetric function approximation). Then, based on this value, a threshold is selected that allows rejecting as many events with a 'false' axis as possible and preserving the maximum number of true ones. The errors of the method as a function of the primary particle mass and energy are shown in Fig. 2. It can be seen that despite the high quality of the filtering (partly due to the higher relative contribution of lighter particles (p) and low energies (1–5 PeV) to the total error), the errors of the method depend on the parameters of the primary particle.

Thus, it is reasonable to develop a neural network method for reliable filtering of 'false' maxima events with minimal dependence on the energy, mass and angle of arrival of the primary particle.

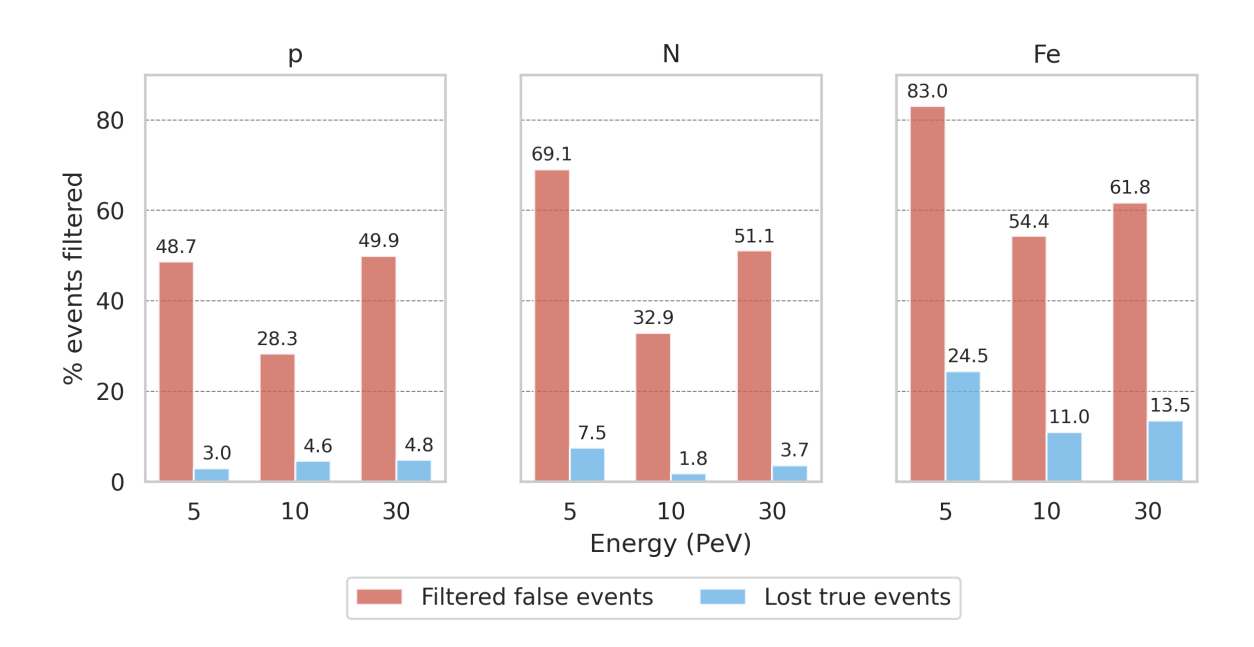


Figure 2. Performance of the classical approach to filtering maxima base on the quality of approximation by an axially symmetric function.

#### 4. DATA SIMULATION

To develop and test the filtering methods, we generated an extensive model database of EAS images using the computational resources of the Lomonosov supercomputer [9]. The simulation was carried put for three fixed energies (5, 10, 30 PeV), three types of primary particles (proton (p), nitrogen (N), iron (Fe)) and three zenith angles (15°, 20°, 25°), the QGSJETII-04 [10] hadron interaction model was used. The telescope height was fixed at 500 m. The CORSIKA [11] and Geant4 [12] software packages were used to simulate the development of the shower and the passage of photons through the optical scheme of the telescopes.

For each combination of parameters, many realizations of cascades were generated, taking into account statistical fluctuations in the development of the showers. Each cascade was also reused multiple times for uniform filling of the simulated field of view. All methods described below were trained on the same training set, across all its examples. Similarly, the same test set was used for testing all methods. A total of 18 000 images were used for training, and 9 000 for testing.

The images were processed to reconstruct the shower axis position by fitting the distribution of Cherenkov photons with an axis-symmetric function [7]. Events in which the reconstructed axis location deviated by more than 25 m from the true value were labeled as false maxima. The analysis showed that when the true axis was within the detector's FOV, the method almost

Table 1. CNN Architecture

	Table 1. Civit Themsecoure					
Layer	Type	Kernel	Stride	Out Channels		
conv1	Conv2d	3×3	1	2		
conv2	Conv2d	$4\times4$	2	6		
conv3	Conv2d	$4\times4$	2	3		
conv4	Conv2d	$4 \times 4$	4	3		
fc1	Linear	_	_	1		

always reconstructed the axis position correctly. However, in cases where the axis was located near or beyond the FOV edge, the algorithm performed poorly. Therefore, we reformulated the task as the identification of whether the EAS axis is located within the detector's FOV.

So, in this work it is considered that 'true' images correspond to the situation when the shower axis lies inside the telescope's FOV, 'false' — when it does not. For a telescope altitude of 500 m, this boundary will lie approximately at 180 m: events in the simulation of which the shower axis fell further than 180 meters will be called 'false'.

The ratio of true to false events in this simulation setup was approximately 1:3.

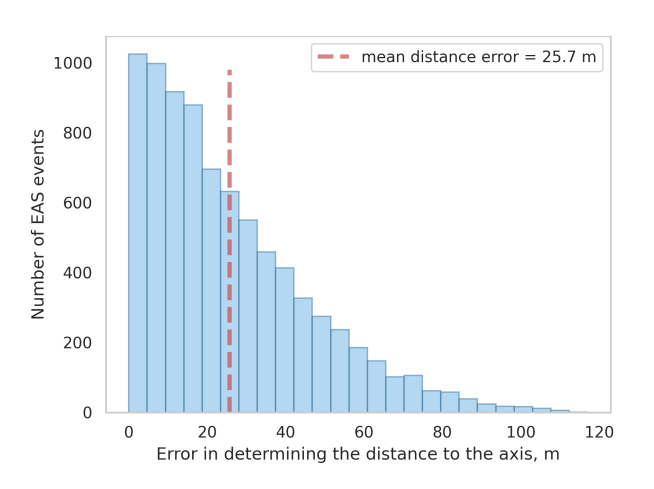
## 5. METHOD

## 5.1. Method 1 - Regression of the Distance to the EAS Axis

The first proposed approach is based on regressing the distance from the center of the telescope's FOV to the projected shower axis using a convolutional neural network (CNN) [13]. The network architecture includes several convolutional blocks with ReLU [14] activation functions, and a fully connected output layer that predicts the scalar distance, as detailed in table 1. The training was performed using the MSE loss function with synthetic data where the true distance to the axis is known.

To classify events based on the regression results, a distance threshold was introduced, above which events were classified as 'false'. The threshold optimization was carried out to maximize filtering accuracy while minimizing losses of true events. The most effective threshold was found to be 210 m, which suppresses 71% of false events while losing only 2.3% of true events (Fig. 3). The analysis showed that the optimal threshold is virtually independent of the primary particle mass and changes only slightly with energy (see Fig. 4), confirming the universality of the

approach.



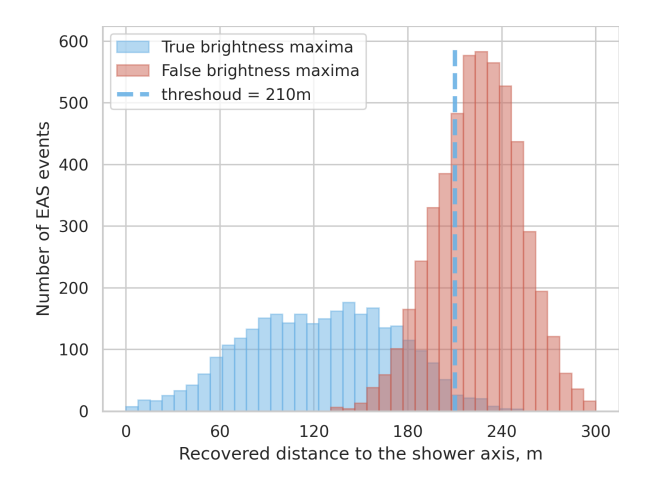


Figure 3. On the left are regression errors for reconstructing the distance to the true shower axis. On the right is the reconstructed distance for two classes of events — true and false. For a telescope height of 500 m, a distance of 180 m from the telescope axis corresponds to the real position of the FOV boundary.

## 5.2. Method 2 — Autoencoder with Spatial Transformer Network

The second approach is based on the use of an autoencoder [15], trained to reconstruct true EAS images. The model architecture includes a preliminary Spatial Transformer Network (STN, [16]) block that learns the optimal transformation of the input image (including rotation and scaling) to normalize the orientation and position of the Cherenkov light spot. The presence of the STN block turns out to be extremely important for the autoencoder due to the different possible positions of the light spot on the mosaic: without preliminary transformation, the autoencoder would have to learn the shape of the image for each set of coordinates of the shower axis incidence. The STN-block parameters are given in table 2, the autoencoder parameters are in table 3.

The autoencoder was trained using the standard MSE loss for true events, and for false events, a negative contribution to the loss function was added, encouraging an increase in the reconstruction error. The reconstruction error (MSE between the original and reconstructed images) was used as a feature for classification. Although the autoencoder alone demonstrated lower efficiency compared to CNN (see Fig. 5), it has a different error nature, opening the possibility of useful contamination of the two methods.

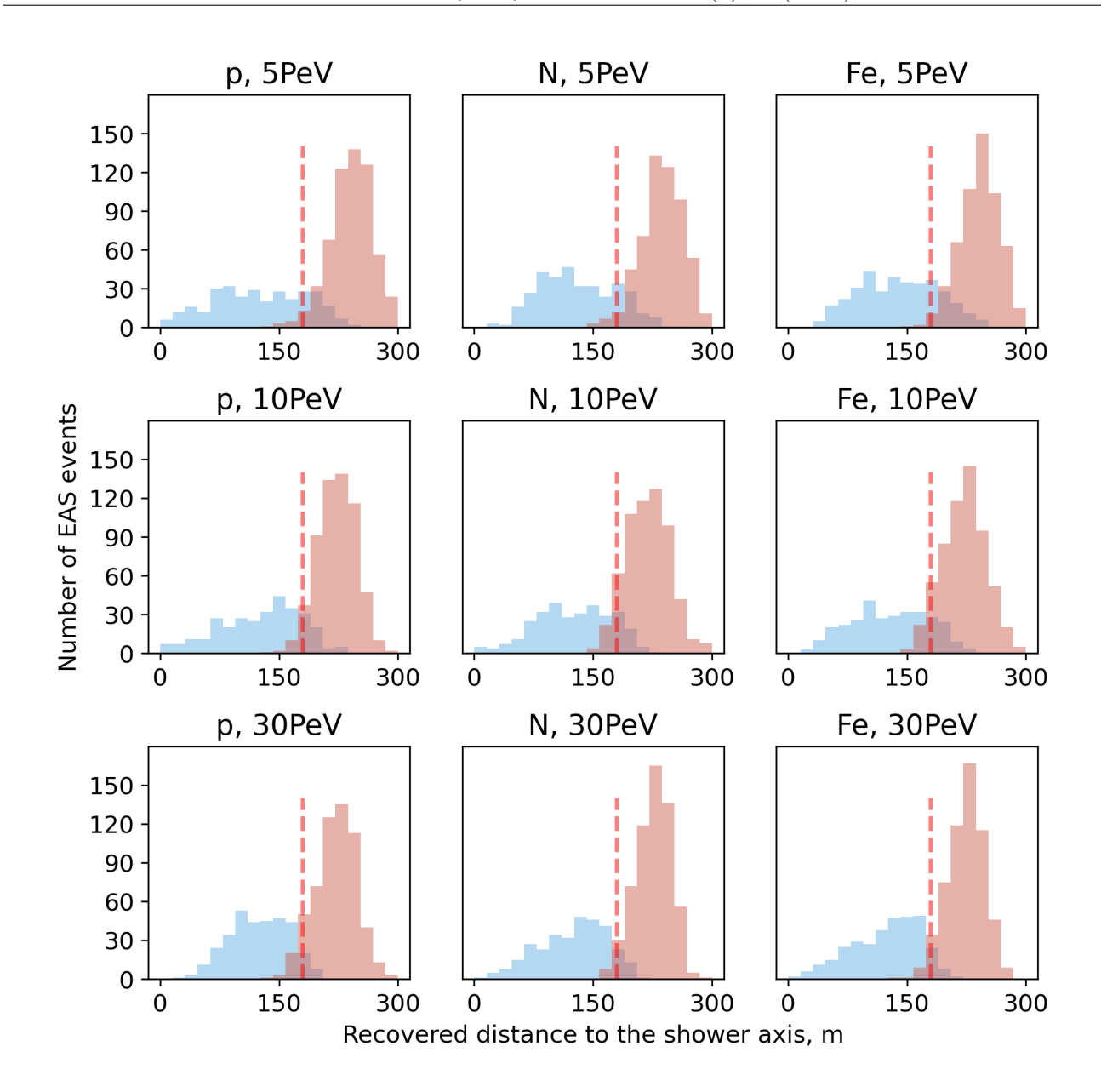


Figure 4. Dependence of the separation boundary on the mass (type) and energy of the primary particle.

# 5.3. Combination of Methods

The combination of the two methods is implemented in a straightforward manner by using their outputs as independent features. In our case, we adopted a linear decision boundary. Although more complex nonlinear classifiers could, in principle, provide slightly higher precision, the gain was found to be negligible compared to the simplicity and interpretability of the linear approach. The optimal decision boundary was determined using logistic regression with class weights (2:1 for 'true' vs. 'false' images to address imbalance). The model learned a linear separator of the form

$$15.68 \cdot |R| + 3.46 \cdot \zeta - 12.05 = 0$$

Table 2	STN Module Architectu	re

Layer	Type	Kernel/	Stride	
	<i>J</i> 1	Units		
stn.conv1	Conv2d	$5 \times 5$	1	
stn.pool1	MaxPool2d	$2\times2$	2	
stn.conv2	Conv2d	$5 \times 5$	1	
stn.pool2	MaxPool2d	$2\times2$	2	
stn.fc1	Linear	32	_	
stn.fc2	Linear	6	_	

Table 3. Autoencoder Architecture.

Layer	Type	Kernel/Units	Stride
enc.1	Conv2d	$3\times3$	2
enc.2	Conv2d	$3\times3$	2
enc.3	Conv2d	$3\times3$	2
neck.1	Linear	128	_
neck.2	Linear	1600	_
dec.1	Deconv2d	$3\times3$	2
dec.2	Deconv2d	$3\times3$	2
dec.3	Deconv2d	$3\times3$	2

where |R| denotes the recovered distance and  $\zeta$  represents the reconstruction error (MSE). The optimal decision boundary and the final AUC of separation are shown in Fig. 6.

# 6. RESULTS

Table 4 shows the results of the combined 'false' maxima filtering method compared to the classical method. It is shown that the method achieves higher accuracy for the selected primary particle type and energy. We also provide a diagram in Fig. 7 similar to Fig. 2 to illustrate the extremely weak dependence of the method errors on the primary particle mass and energy in the claimed range of values.

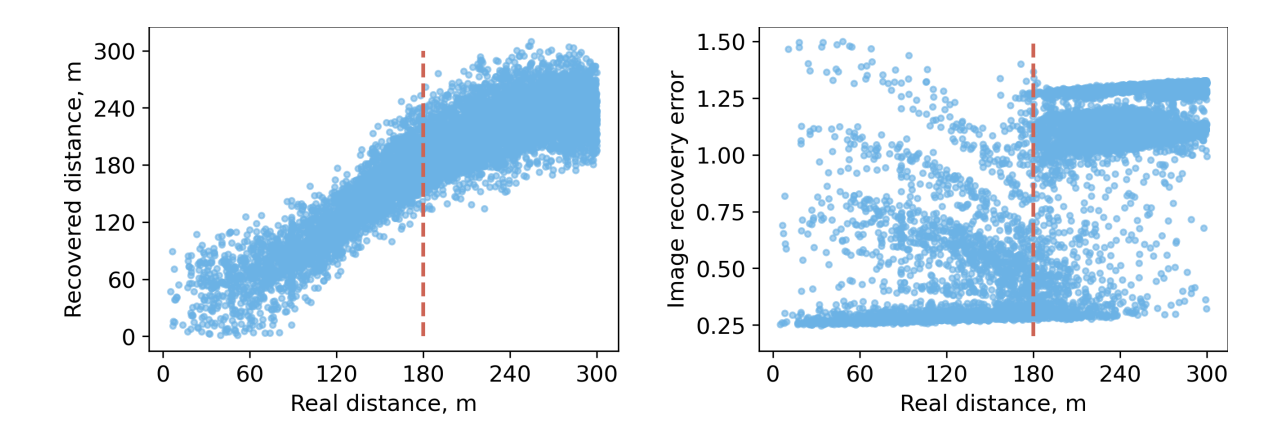


Figure 5. Dependence of the feature used for classification on the true distance for both proposed architectures: on the left for CNN, on the right for the autoencoder. The red line at 180 meters shows the boundary of the telescope's field of view (for an altitude of 500 m), events to the left of this boundary are true, to the right are false. It can be seen that distance regression gives a smaller and better interpretable error, while the image restoration error has a more stochastic distribution.

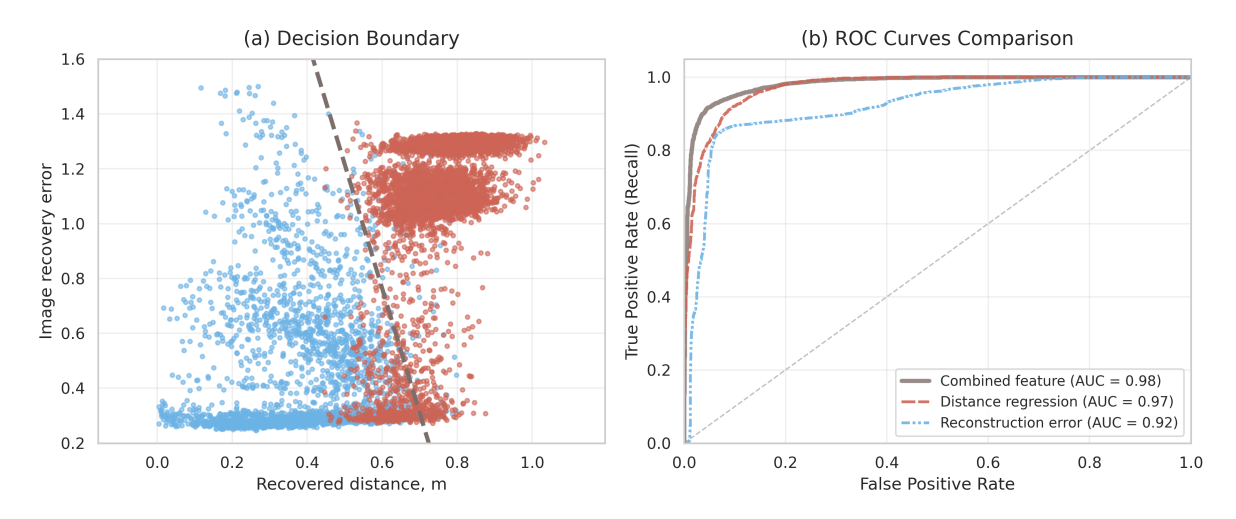


Figure 6. On the left is the combination of features of different methods and the optimal threshold of linear separation for classification. On the right are the resulting ROC curves of the described methods.

## 7. DISCUSSION

The results demonstrate that the combination of CNN-based regression and the autoencoder with a spatial transformer effectively suppresses false brightness maxima in EAS images without the need for adjustments based on specific primary particle parameters. This makes the method particularly promising for integration into the online or offline data processing system of the SPHERE-3 experiment.

It should be noted that the training was conducted exclusively on model data, which requires further validation taking into account electronics noise, SiPM crosstalk and digitization effects.

TD 1.1 4 D C	•	1 4	1 1	1	1	41 1	/ 1 ·	047
Table 4. Performance	comparison	between	classical	and	suggested	methods	(values in	%).

Particle	Energy	Energy, Filtered False			Lost True		
	PeV	Classical	Ours $(\Delta)$	Classical	Ours $(\Delta)$		
p	5	48.66	93.51 (+44.85)	2.97	4.51 (+1.54)		
	10	28.27	86.36 (+58.09)	4.60	$0.66 \; (-3.94)$		
	30	49.93	93.51 (+43.58)	4.78	<0.01 (-4.78)		
N	5	69.09	91.86 (+22.77)	7.52	3.74 (-3.78)		
	10	32.90	90.32 (+57.42)	1.83	2.31 (+0.48)		
	30	51.10	88.34 (+37.24)	3.66	<0.01 (-3.66)		
Fe	5	83.04	91.31 (+8.27)	24.46	$4.62 \; (-19.84)$		
	10	54.35	93.51 (+39.16)	10.99	3.08 (-7.91)		
	30	61.76	89.00 (+27.24)	13.53	0.22 (-13.31)		

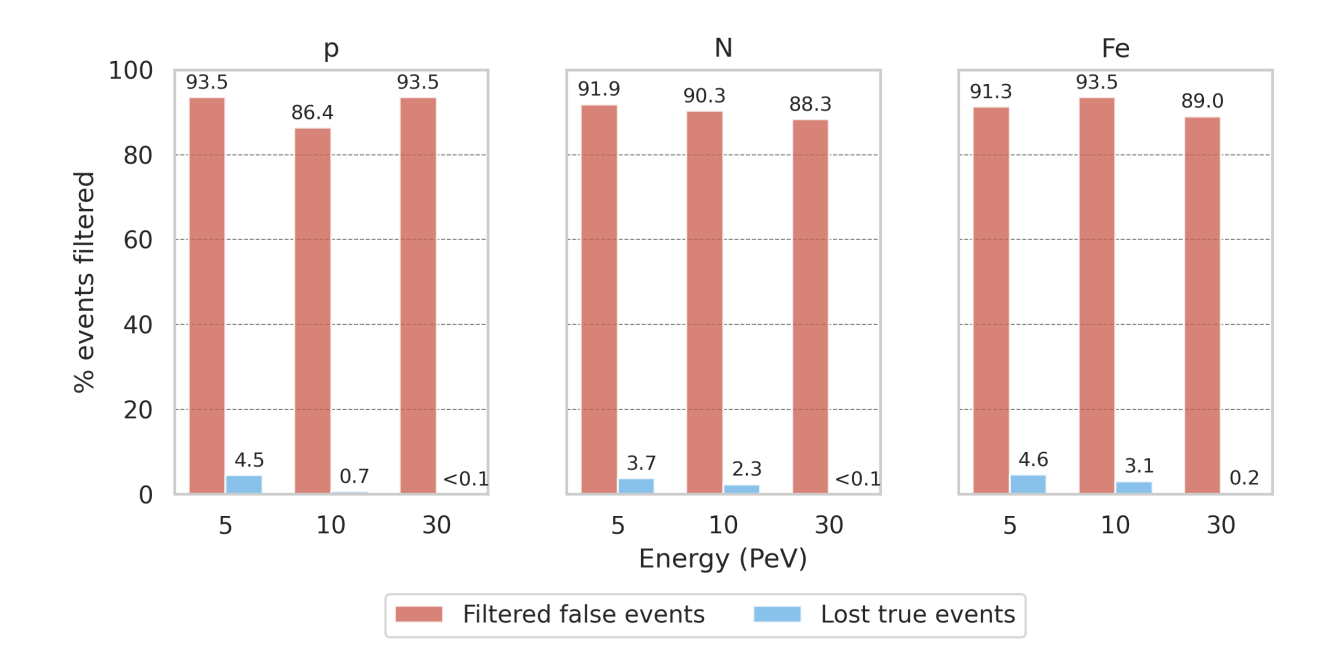


Figure 7. Neural network combined 'false' maxima filtration performance.

An additional direction for development is the adaptation of the approach to the variable flight altitude, taking into account the influence of background photons and decreasing the sensibility of the method to changes in the telescope operation parameters and conditions.

## ACKNOWLEDGMENTS

The study was conducted under the state assignment of Lomonosov Moscow State University.

## **FUNDING**

This work is supported by the Russian Science Foundation under Grant No. 23-72-00006, (https://rscf.ru/project/23-72-00006/).

#### CONFLICT OF INTEREST

The authors of this work declare that they have no conflicts of interest.

- [1] J. Abraham, P. Abreu, M. Aglietta et al. NIM A 613, 29 (2010) https://doi.org/10.1016/j.nima.2009.11.018
- [2] The Telescope Array Collaboration // arXiv:2406.08612 [astro-ph.HE] https://doi.org/10.48550/arXiv.2406.08612
- [3] A. A. Ivanov, A. D. Krasilnikov, M. I. Pravdin, A. V. Sabourov // Astropart. Phys. 6, 1 (2015) http://doi.org/10.1016/j.astropartphys.2014.07.002
- [4] D. V. Chernov, C Azra, E. A. Bonvech et al. // Phys. At. Nucl. 85(6), 641 (2022)
- [5] R. A. Antonov, T. V. Aulova, E. A. Bonvech et al. // Phys. Part. Nucl. 46(1), 60 (2015).
   https://doi.org/10.1134/S1063779615010025
- V. I. Galkin, C. G. Azra, E. A. Bonvech et al., Moscow Univ. Phys. Bull. 79 (Suppl 1), 384 (2024).
   https://doi.org/10.3103/S002713492470111X
- [7] E. A. Bonvech, N. O. Ovcharenko, O. V. Cherkesova, et al., Bull. Russ. Acad. Sci. Phys. 89, 1007 (2025). https://doi.org/10.1134/S1062873825711572
- [8] V. A. Ivanov, V. I. Galkin, E. A. Bonvech et al., https://doi.org/10.48550/arXiv.2410.14921
- [9] V. Voevodin, A. Antonov, D. Nikitenko et. al., Supercomputing Frontiers and Innovations 6(2), 4(2019) https://doi.org/10.14529/jsfi190201
- [10] S. Ostapchenko, Nucl. Phys. B Proc. Suppl. 151, 143 (2006). https://doi.org/10.1016/j.nuclphysbps.2005.07.026
- [11] D. Heck, J. Knapp, J.N. Capdevielle, et al., FZKA-6019. (1998).

- [12] S. Agostinelli, J. Allison, K. Amako, et al., NIMA. 506(3), 250 (2003). https://doi.org/10.1016/S0168-9002(03)01368-8.
- [13] Y. LeCun, K. Kavukcuoglu, C. Farabet, Proc. of 2010 IEEE Int. Symp. on Circuits and Systems. 253 (2010). https://doi.org/10.1109/ISCAS.2010.5537907
- [14] V. Nair, G. E. Hinton, Proc. of the 27th Int. Conf. on Machine Learning (ICML-10). 807 (2010). http://www.cs.toronto.edu/fritz/absps/reluICML.pdf
- [15] D. E. Rumelhart, G. E. Hinton, R. J. Williams // Nature **323**, 533 (1986). https://doi.org/10.1038/323533a0
- [16] M. Jaderberg, K. Simonyan, A. Zisserman, et al., https://doi.org/10.48550/arXiv.1506.02025